JOURNAL OF SOLID STATE CHEMISTRY 94, 106–120 (1991)

Thermodynamic Stability of Perovskites and Related Compounds in Some Alkaline Earth–Transition Metal–Oxygen Systems

HARUMI YOKOKAWA,* NATSUKO SAKAI, TATSUYA KAWADA, AND MASAYUKI DOKIYA

National Chemical Laboratory for Industry, Tsukuba Research Center, Ibaraki-305, Japan

Received December 19, 1990

The thermodynamic properties of some alkaline earth (A)–transition metal (M) perovskites and K_2NiF_4 compounds have been collected, analyzed, and utilized to examine their stabilities by constructing the chemical potential diagrams of a log $[a(A)/a(M)]$ vs log $P(O_2)$ plot. A thermodynamic analysis was performed on the dissociation reaction of K_2NiF_4 compounds (A_2MO_4) into perovskites (AMO_3) and alkaline earth oxides (AO) using empirical correlations between stabilization energy and tolerance factor. It has been found that the softness of calcium ions, which shrink markedly with decreasing coordination number from 12 to 9, makes the calcium K_2NiF_4 compounds (Ca_2MO_4) relatively less stable with increasing radius of the transition metal ions, $r(M^{4+})$. This destabilization related to the coordination-number-dependent radii implies that when compared with the strontium perovskites, the calcium analogous perovskites may have a smaller number of oxygen vacancies, because the formation of oxygen vacancies should be accompanied with a decrease in coordination number of A-site ions.

I. Introduction

Perovskites and K_2NiF_4 compounds have recently attracted much attention because they exhibit a variety of magnetic, electrical, and other properties (*1–9*). Their interesting features from the materials chemistry viewpoint are (i) formation of a series of Ruddlesden–Popper phases, $A_nM_nO_{3n}$-AO (n = 1, 2, . . .) (*10*), (ii) a wide range of substitutional solid solutions, and (iii) a variety of lattice defects (*6*).

Since the thermodynamic properties associated with these features are quite important in optimizing materials selection, we have taken chemical thermodynamic considerations of the stability of those perovskites which are technologically important in a high temperature solid oxide fuel cell (*11–16*). In the present paper, the alkaline earth–transition metal–oxygen systems are examined with the following three approaches:

(i) The thermodynamic properties of perovskites and other double oxides have been collected and evaluated; on the basis of these data, chemical potential diagrams at a selected temperature have been constructed to show their relative stabilities in a visually clear manner.

(ii) An attempt has been made to find respective empirical correlations for perovskites and K_2NiF_4 compounds between thermodynamic functions and ionic radii.

* To whom correspondence should be addressed.

0022-4596/91 $3.00

TABLE I

THERMODYNAMIC CONSTANTS OF THE ALKALINE EARTH-TITANATES

Compound	State	Functions at 298.15 K $\Delta_f H$ (kJ/mole)	$\Delta_f G$ (kJ/mole)	S (J/K mole)	Coefficient of heat capacity eq. (J/K mole) a	b	c	Temp. limit T (K)		$\Delta_{tr} H$ (kJ/mole) (Ref.)
$CaTiO_3$	c1	−1660.6	−1575.2	93.64	127.49	5.69	−27.99	1530(tp)	2.30	HGS (*17*),
	c2				134.01			2188(mp)		Cp (*18*)
$Ca_3Ti_2O_7$	c	−4003.9	−3804.6	234.7	299.24	15.9	−57.24	1998(mp)		HGS (*24, 17*)
$Ca_4Ti_3O_{10}$	c	−5671.6	−5387.1	328.4	424.05	21.59	−82.38	2028(mp)		24
$SrTiO_3$	c	−1672.4	−1588.4	108.8	118.11	8.54	−19.16	2183(mp)		HGS (*17*), Cp (*18*)
Sr_2TiO_4	c	−2287.4	−2172.4	159.0	160.87	16.07	−19.54	2130(dp)		HGS (*17*)
$Sr_3Ti_2O_7$	c	−3969.7	−3769.0	262.55	278.98	24.61	−38.70	1853(dp)		est.
$Sr_4Ti_3O_{10}$	c	−5648.4	−5362.7	367.95	397.09	33.15	−57.86	1853(dp)		24, est.
$SrTi_{12}O_{19}$	c	−9847.4	−9298.6	527.08	935.9	27.57	−293.44	2500		est.
$BaTiO_3$	c1	−1659.8	−1572.3	107.9	125.85	5.52	−26.501	394.65(tp)	.201	HGS (*17*),
	c2				125.85	5.52	−26.501	1773(mp)	0	Cp (*23*)
	c3				134.9			1889(mp)		Cp (*23*)
										Cp (*23*)
Ba_2TiO_4[a]	c	−2243	−2133	196.6	181.79	9.87	−34.803	2133(mp)		HGS (*17*)

[a] Not K_2NiF_4-type.

TABLE II

THERMODYNAMIC CONSTANTS OF THE ALKALINE EARTH ZIRCONATES AND HAFNATES

Compound	State	Functions at 298.15 K $\Delta_f H$ (kJ/mole)	$\Delta_f G$ (kJ/mole)	S (J/K mole)	Coefficient of heat capacity eq. (J/K mole) a	b	c	Temp. limit T (K)	$\Delta_{tr} H$ (kJ/mole) (Ref.)
$CaZrO_3$	c	−1766.9	−1681.1	100.08	119.24	12.05	−21.00	2613(mp)	HGS (*17*), Cp (*21*)
$SrZrO_3$	c	−1767.3	−1682.8	115.1	121.25	12.22	−21.615	2923(mp)	HGS (*17*), Cp (*21*)
$Sr_4Zr_3O_{10}$	c	−5906.2	−5622.4	399.7	410.0	47.02	−68.50	2475(dp)	est.
$Sr_3Zr_2O_7$	c	−4136.4	−3937.2	284.6	289.42	34.80	−46.78	2475(dp)	est.
Sr_2ZrO_4	c	−2364.6	−2250.0	169.5	167.97	22.58	−25.16	2600(mp)	est.
$BaZrO_3$	c	−1779.5	−1694.5	123.7	122.80	8.79	−21.97	2000	HGS (*17*), Cp (*21*)
Ba_2ZrO_4	c	−2351.0	−2239.6	201.2	170.68	21.46	−23.80	2000	est.
$CaHfO_3$	c	−1811.7	−1728.5	113.39	120.92	13.56	−19.46	2000	H (*17*), est.
$SrHfO_3$	c	−1814.6	−1727.1	110.	122.2	13.8	−19.87	1900	HGS (*17*), Cp (*21*)
Sr_2HfO_4	c	−2413.3	−2300.0	178.1	168.97	25.07	−22.80	2000	est.
$BaHfO_3$	c	−1832.2	−1745.2	122.2	123.8	13.4	−17.36	1500	HGS (*17*)
Ba_2HfO_4	c	−2401.1	−2291.2	210.2	170.33	25.53	−20.82	2000	est.

TABLE III
THERMODYNAMIC CONSTANTS OF STRONTIUM VANADIUM OXIDES

Compound	State	Functions at 298.15 K $\Delta_f H$ (kJ/mole)	$\Delta_f G$ (kJ/mole)	S (J/K mole)	Coefficient of heat capacity eq. (J/K mole) a	b	c	Temp. limit T (K)	$\Delta_{tr}H$ (kJ/mole) (Ref.)
SrV_2O_6	c	−2362.7	−2204.7	195.2	214.74	29.34	−22.86	1000	est.
$Sr_2V_2O_7$	c	−3126.7	−2940.2	254.6	264.59	36.09	−48.29	1200	HGS (*17*), Cp (est)
$Sr_3V_2O_8$	c	−3796.7	−3591.7	324.0	314.44	42.84	−54.15	1500	est.
$SrVO_3$	c	−1444.6	−1363.6	117.15	122.28	16.01	−19.44	2000	est.
Sr_2VO_4	c	−2054.6	−1943.7	171.55	172.13	22.76	−25.30	2000	est.

Such correlations make it possible to thermodynamically explain why some A_2MO_4 phases do not exist despite some crystal chemical allowance. Estimates of the thermodynamic functions of such nonexistent compounds are important to predict the composition range of solid solutions.

(iii) Discussion has been made on the relation between the appearance of Ruddlesden–Popper phases and the extent of oxygen nonstoichiometry in perovskite phases; both properties should be closely related to changes in stabilization energy when the coordination number of A-site ions decreases.

II. Thermodynamic Data and Chemical Potential Diagrams

Thermodynamic properties of binary oxides are generally taken from major databooks (*17–27*). The thermodynamic data of double oxides listed in Tables I to IV were taken from the databooks as well as experimental results (*9, 28–40*); intermetallic compounds and liquid alloys were neglected because our primary concern is on double oxides. After thermodynamic data were evaluated or estimated, the chemical potential diagrams were constructed using a com-

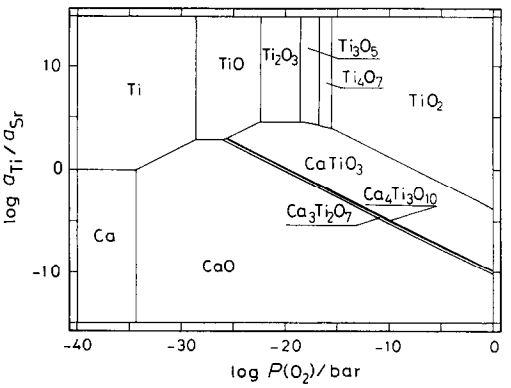

FIG. 1. Chemical potential diagram of the Ca–Ti–O system at 1473 K.

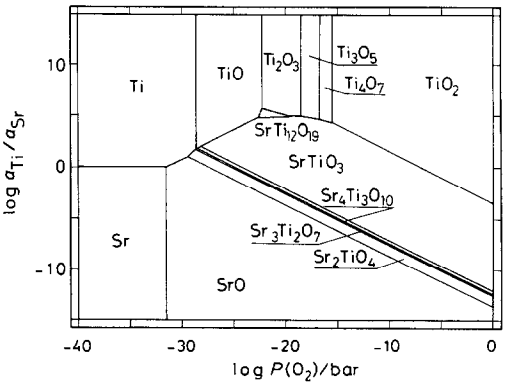

FIG. 2. Chemical potential diagram of the Sr–Ti–O system at 1473 K.

TABLE IV

THERMODYNAMIC CONSTANTS OF THE ALKALINE EARTH-MOLYBDATES AND TUNGSTATES

Compound	State	Functions at 298.15 K $\Delta_f H$ (kJ/mole)	$\Delta_f G$ (kJ/mole)	S (J/K mole)	Coefficient of heat capacity eq. (J/K mole) a	b	c	Temp. limit T (K)	$\Delta_{tr}H$ (kJ/mole) (Ref.)
$CaMoO_3$	c	−1265.0	−1179.0	90.0	104.28	32.61	−13.51	2000	HGS (*34*), est.
$CaMoO_4$	c	−1541.4	−1434.7	122.6	133.72	29.20	−22.34	1000	HGS (*17, 21*)
$SrMoO_3$	c	−1280.0	−1194.9	103.0	103.0	35.22	−10.88	2000	H (*17, 34*)
Sr_2MoO_4	c	−1878.6	−1763.6	157.4	153.50	41.97	−16.74	2500	35
$SrMoO_4$	c	−1548.	−1443.	140.0	134.14	29.37	−22.95	1731(mp)	H (*17, 21*)
Sr_3MoO_6	c	−2772.0	−2607.5	248.8	213.78	42.87	−34.67	1900(dp)	Est.
$BaMoO_3$	c	−1234.0	−1152.3	125.7	104.39	35.45	−9.89	2500	H (*17, 21*)
$BaMoO_4$	c	−1548.	−1439.7	138.	132.67	29.04	−23.70	1720	HGS (*17, 21*)
Ba_2MoO_5	c	−2145.0	−2009.6	216.02	183.20	36.02	−28.57	1573(dp)	est.
Ba_3MoO_6	c	−2730.0	−2567.3	286.4	233.73	43.0	−33.44	1820(mp)	est.
$CaWO_4$	c	−1645.2	−1538.5	126.4	134.56	20.69	−24.44	1853(mp)	HGS (*17, 21*)
Ca_3WO_6	c	−2930.5	−2758.4	195.0	236.52	29.72	−38.33	2523(mp)	(*21*)
$SrWO_4$	c	−1643.7	−1535.9	133.5	137.47	22.98	−23.29	1808(mp)	(*38*)
Sr_2WO_5	c	−2303.0	−2159.3	167.8	187.29	29.73	−29.15	2000	(*38*)
Sr_3WO_6	c	−2928.1	−2753.4	218.8	237.11	36.48	−35.01	2000	(*38*)
$BaWO_4$	c	−1685.4	−1580.1	152.22	138.18	23.21	−22.30	1748(mp)	(*39*)
Ba_2WO_5	c	−2378.5	−2239.1	202.94	188.71	30.19	−27.17	2000	(*39*)
Ba_3WO_6	c	−3024.5	−2855.5	269.26	239.24	37.7	−32.04	2068(mp)	(*39*)

puter program, CHD (*12, 13*). A log $[a(A)/a(B)]$ vs log $P(O_2)$ plot is adopted in the present investigation. Diagrams for some alkaline earth (mainly strontium)–transition metal–oxygen systems are presented in Figs. 1–5 to see how the stability of perovskites and related phases changes among some transition metal systems.

III. Stability of Perovskites and K_2NiF_4 Compounds

The thermodynamic stability of double oxides should be examined at least on the following two aspects: the stabilization en-

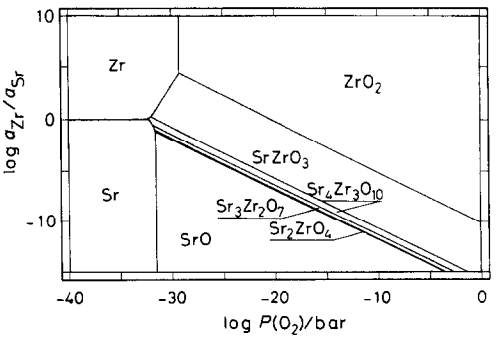

FIG. 3. Chemical potential diagram of the Sr–Zr–O system at 1473 K.

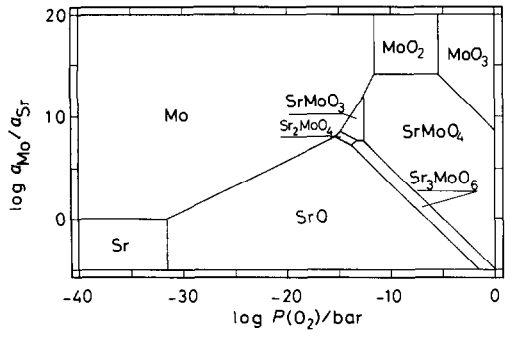

FIG. 4. Chemical potential diagram of the Sr–Mo–O system at 1473 K.

ergy from constituent binary oxides and the chemical thermodynamic stability against any dissociation reactions.

The enthalpies of formation of double oxides from their constituent binary oxides have been discussed so far in terms of ionic radius, charge, polarizability, and their related factors. It is therefore of interest to extract a dominant factor that determines stability of the particular crystal structure for selected compounds. Actually, attempts to sort various crystal structures using chemical or physical scales have been made with great success (*41–43*). Even so, such sorting maps are not appropriate to explain why certain compounds are unstable. It is therefore of great interest to make chemical thermodynamic considerations on this problem using chemical scales similar to those used in structure sorting maps.

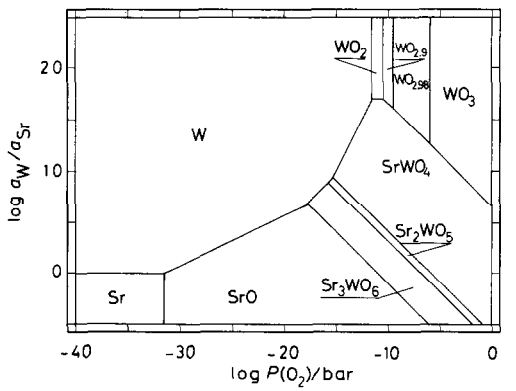

FIG. 5. Chemical potential diagram of the Sr–W–O system at 1473 K.

Since ionic radius is a good scale for sorting ionic crystal structures (*44*), many attempts have been made to correlate the enthalpy of formation with physical properties derived from ionic radii (*45*). For perovskites, the tolerance factor is one of the most appropriate measures for scaling enthalpy and entropy (*8, 9, 46, 47*). We actually found that the stabilization energy of perovskites becomes large when the tolerance factor is nearly equal to unity (*16*).

In the present investigation, (i) an attempt has been made to examine the stability of perovskites against disproportionation reaction and (ii) an attempt has been made also to derive a similar correlation for K_2NiF_4 compounds; together with the correlation for perovskites, this makes it possible to examine relative stabilities among Ruddlesden–Popper phases.

Stability of Perovskites

The enthalpy of formation of perovskites, AMO_3, from AO and MO_2 can be given empirically as

$$\delta_P = \Delta_f H^\circ(AMO_3) - \Delta_f H^\circ(AO) - \Delta_f H^\circ(MO_2) \quad (1)$$

$$= 2[-\alpha_P + \beta_P(1 - t_P)]. \quad (2)$$

Here t_P is the tolerance factor which can be evaluated merely from ionic radii as

$$t_P = (r_A(\mathrm{XII}) + r_O)/\sqrt{2}(r_M(\mathrm{VI}) + r_O) \quad (3)$$

for perovskites, where $R_A(\mathrm{XII})$, $r_M(\mathrm{VI})$, r_O are radii for A-site cations with 12 coordinates, for B-site cations with 6 coordinates, and for oxide ions, respectively. Using Shannon's radii (*49*), the following numerical correlation can be derived for $A^{II}M^{IV}O_3$ perovskites (*16*):

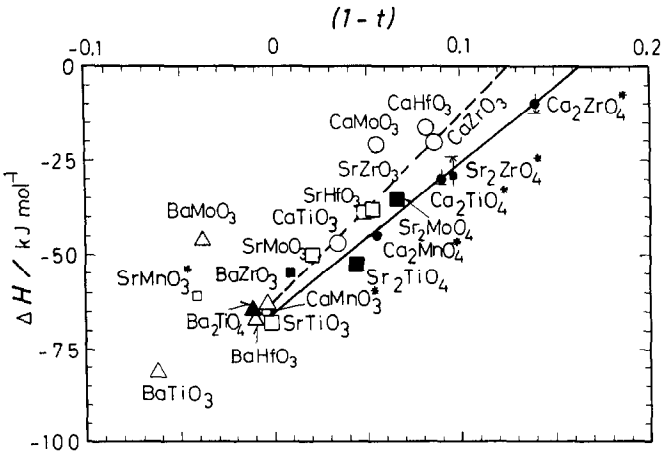

FIG. 6. The enthalpy of formation of perovskites and K_2NiF_4 compounds from AO and BO_2 per mole of metallic element: Large symbols are experimental values, small ones being estimates derived from the examination of phase relations; open and solid symbols are for perovskites and K_2NiF_4 compounds, respectively.

$$\delta_P = 2[-60 + 500(1 - t_P)] \text{ kJ mole}^{-1}. \quad (4)$$

This correlation is shown in Fig. 6 for some alkaline earth transition metal oxygen systems.

When comparison is made among the Sr–M–O (M = Zr, Mo, W) systems in how the stability field of perovskites appears in the chemical potential diagrams, it can be clarified that the stability of perovskites cannot be determined merely by the stabilization energy (Eq. (4)) but requires other thermodynamic factors; $SrMoO_3$ and $SrZrO_3$ have essentially the same magnitude of the stabilization energy, whereas they exhibit quite different features of stability polygons (compare Figs. 3 and 4). Roughly speaking, the stable region of oxygen potential for double oxides is primarily determined by the stability of the less stable constituent oxide. Usually the alkaline earth oxides are quite stable against reduction; this suggests that the stable oxygen potential region of perovskites is governed, to the first order of approximation, by the chemical thermodynamic nature of the transition metal binary oxides.

As a first example, the Sr–Mo–O system is considered: in the Mo–O subsystem, there exists an MoO_3 phase in addition to the MoO_2 phase. Note that double oxides with Mo^{6+} are quite stable; for example, the enthalpy change for the following reaction is about -210 kJ/mol:

$$SrO + MoO_3 = SrMoO_4. \quad (5)$$

This large stabilization of $SrMoO_4$ makes narrow the stability area of $SrMoO_3$. That is, the equilibrium pressure for the reaction

$$SrMoO_4 = SrMoO_3 + \tfrac{1}{2}O_2(g) \quad (6)$$

is much lower than that for the coresponding MoO_2/MoO_3 equilibrium.

In the Sr–W–O system, no perovskite nor K_2NiF_4 compound is reported so far. The present considerations on stability of perovskites can explain why the AWO_3 (A = alkaline earth) perovskite is not reported. Using Eq. (4), the enthalpy of formation of $SrWO_3$

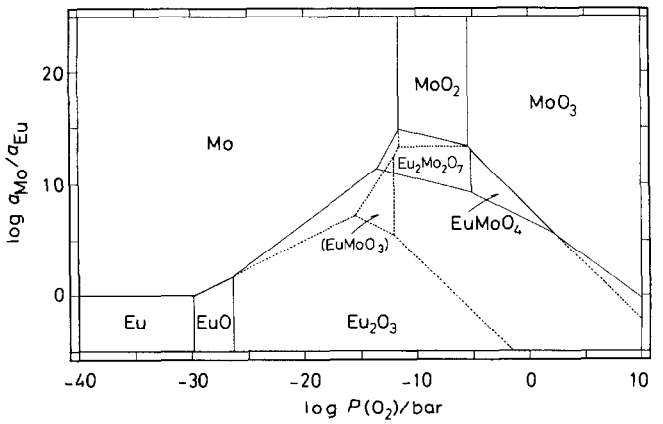

FIG. 7. Estimated chemical potential diagram of the Eu–Mo–O system at 1473 K including an unstable $EuMoO_3$ phase.

can be estimated. This estimate leads to the Gibbs energy change for the following reaction as -21.0 kJ/mol:

$$SrWO_3 = \tfrac{2}{3}SrWO_4 + \tfrac{1}{3}W + \tfrac{1}{3}SrO. \quad (7)$$

Figure 5 shows that the stability of WO_2 itself is quite narrow compared with WO_3 or W and this makes the perovskite phase unstable.

A similar consideration can be applied to the Eu–Mo–O system. Since the ionic radius of Eu^{2+} is essentially the same as that of Sr^{2+}, the Eu(II)–molybdenum perovskite can be expected to have a relatively large stabilization energy; however, an attempt to synthesize this phase was not successful (*19*). This can be thermodynamically explained as follows: Fig. 7 shows the estimated chemical potential diagram for the Eu–Mo–O system. The thermodynamic properties of $EuMoO_3$ and $EuMoO_4$ were estimated so as to have the same stabilization energy as $SrMoO_3$ and $SrMoO_4$, respectively. When the Eu(III) compounds are neglected, the calculated chemical potential diagram is quite similar to that of the Sr–Mo–O system. In the Eu–Mo–O system, however, a pyrochlore phase, $Eu(III)_2Mo_2O_7$, exists in a reducing atmosphere. The stabilization energy of $Eu(III)_2Mo_2O_7$ was estimated as an averaged value between $La_2Zr_2O_7$ (*25*) and $Lu_2V_2O_7$ (*13*), because these three pyrochlores have essentially the same ionic radius ratio, $(r_A + r_O)/(r_B + r_O) = 1.20$. As shown in the three-dimensional chemical potential diagram given in Fig. 8, the existence of $Eu(III)_2Mo_2O_7$ and Eu_2O_3 phases makes it impossible for $EuMoO_3$ to exist as a stable phase.

Ruddlesden–Popper Phases in A^{II}–M–O and A^{III}–M–O Systems

As seen in Figs. 2–4, Ruddlesden–Popper phases in the A^{II}–M^{IV} system exhibit an interesting parallel arrangement. This should be compared with the A^{III}–M–O system, in which the stability areas of the corresponding phases appear in a sequential manner with decreasing oxygen potential (*12, 13*).

When perovskites and K_2NiF_4 compounds are compared in terms of the stabilization energy from constituent oxides, the following interesting feature can be derived: In the rare earth (Ln)–M–O system, Ln_2MO_4 phases appear even though the stabilization energy is relatively small, whereas

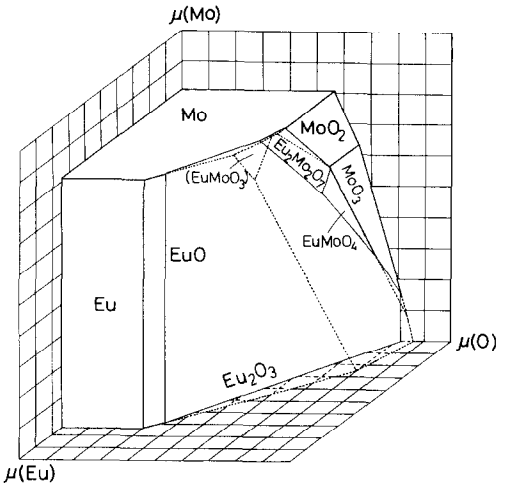

FIG. 8. Three-dimensional chemical potential diagram for the Eu–Mo–O system at 1473 K. The broken line shows how the plane of $EuMoO_3$ is cut off by those of Eu_2O_3 and its compounds.

in some alkaline earth (A)–M–O systems, a A_2MO_4 phase does not stably exist even when some stabilization can be expected from its ionic size matching. For example, the tolerance factors of La_2NiO_4 and La_2CoO_4 are calculated using Shannon's radii (*48*) as 0.875 and 0.859, respectively. The corresponding value, 0.910, or Ca_2TiO_4 implies that the stabilization energy would be large enough for this phase to exist; this is however not the case. Figure 9 shows the appearance of Ruddlesden–Popper phases in the A^{II}–M–O systems. Note that Ca_2MO_4 is absent in many systems.

The absence of K_2NiF_4 compounds can be well explained by the following chemical thermodynamic considerations on dissociation of K_2NiF_4 compounds:

$$A_2MO_4 = AMO_3 + AO. \quad (8)$$

Using the Gibbs energy change of A_2MO_4 and AMO_3 for formation from AO and MO_2, $\Delta_{f,oxide}G^\circ$ (AMO_3) and $\Delta_{f,oxide}G^\circ$ (A_2MO_4), the Gibbs energy change for the above reaction can be written as

$$\Delta_rG^\circ \text{ (eq. 8)} = \Delta_{f,oxide}G^\circ (AMO_3) - \Delta_{f,oxide}G^\circ (A_2MO_4). \quad (9)$$

This suggests that in certain cases, the Gibbs energy change for the dissociation reaction becomes negative, although the Gibbs energy of formation of the K_2NiF_4 compound is itself negative.

This behavior concerning appearance/disappearance of the $A_2^{II}M^{IV}O_4$ phase should be compared with those of the $A_2^{III}M^{II}O_4$ phase. In the A^{III}–M–O system, the valence state in the perovskite phase is different from that in the K_2NiF_4 compound, and the dissociation reaction of $A_2^{III}M^{II}O_4$ is in turn given by the equation

$$2A_2^{III}MO_4 + \tfrac{1}{2}O_2 = 2AMO_3 + A_2O_3, \quad (10)$$

or

$$2A_2^{III}MO_4 + MO + \tfrac{1}{2}O_2 = 2MO_3. \quad (11)$$

This is a combined oxidation–dissociation reaction. In other words, three phases, A_2MO_4, AMO_3, and A_2O_3 (or MO), can coexist in the A^{III}–M–O system, whereas the corresponding three phases cannot coexist in the A^{II}–M–O (AO–MO_2 pseudobinary) systems. This difference is thermodynamically important to explain why La_2MO_4 can exist as a stable phase even though their tolerance factors are usually less than 0.9 and correspondingly their stabilization energies are not high.

Relative Stability among Ruddlesden–Popper Phases

Relative stability of $A_2^{II}MO_4$ to AMO_3 is examined in a more quantitative manner. The tolerance factors for K_2NiF_4 compounds are defined as

$$t_K = (r_A(IX) + r_O)/\sqrt{2}(r_M(VI) + r_O) \quad (12)$$

for K_2NiF_4 compounds, where r_A(IX) is the radius of A-site ions with 9 coordinates, r_M(VI) that of B-site ions with 6 coordinates

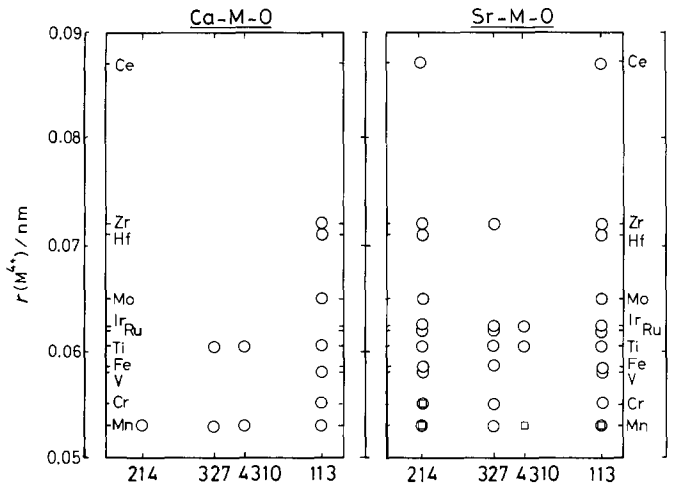

FIG. 9. Appearance of Ruddlesden–Popper phases in the calcium and strontium–transition metal–oxygen systems.

(*48*). A linear relationship can be expected also for K_2NiF_4 compounds between stabilization energy and tolerance factor:

$$\delta_K = \Delta_f H^\circ(A_2MO_4) - 2\Delta_f H^\circ(AO) - \Delta_f H^\circ(MO_2), \quad (13)$$

$$\delta_K = 3[-\alpha_K + \beta_K(1 - t_K)]\ \text{kJ mole}^{-1}. \quad (14)$$

In such a case, the relative stability of A_2MO_4 to AMO_3 (Eq. (8)) can be written using Eq. (4) as

$$\begin{aligned}\Delta_r G^\circ \text{ (Eq. (8))} &= \Delta_{f,\text{oxide}} G^\circ(AMO_3) - \Delta_{f,\text{oxide}} G^\circ(A_2MO_4) \\ &\doteqdot \Delta_{f,\text{oxide}} H^\circ(AMO_3) - \Delta_{f,\text{oxide}} H^\circ(A_2MO_4) \\ &= \delta_P - \delta_K, \quad (15)\end{aligned}$$

where the entropic term, $T\Delta_r S$, of the solid–solid reaction was neglected to the first order of approximation. The relative stability of AMO_3 and A_2MO_4 can be categorized into three cases in terms of their stabilization energies, δ_P and δ_K, as follows: (i) when $\delta_P > \delta_K$, and δ_P, $\delta_K < 0$, both perovskite and A_2MO_4 are stable (case A); (2) when $\delta_P < \delta_K$, and $\delta_P < 0$, only the perovskite is stable (case B); (3) when δ_P, $\delta_K > 0$, neither can exist (case C).

These criteria can be characterized in terms of tolerance factors of perovskite, t_P, and of the K_2NiF_4 compound, t_K. Since α_P and β_P are already given in Eq. (8), determination of α_K and β_K makes it possible to compare stability fields of perovskites and K_2NiF_4 compounds as functions of tolerance factors, t_P and t_K. Figure 10 shows a t_P vs t_K plot for some A–M–O systems. Since the same value of r_B(VI) should be used in deriving t_P and t_K, and since r_A(XII) is usually greater than r_A(IX), t_P is generally greater than t_K in A–B–O systems. The area (A) in the upper part in Fig. 10 corresponds to the field in which both perovskite and K_2NiF_4 phases are stable, whereas in area (B) the K_2NiF_4 phase becomes unstable against the dissociation into AMO_3 and AO.

As a first attempt, we assumed that $\alpha_P = \alpha_K$ and $\beta_P = \beta_K$; this was our previous approximation (*11*). This relation is shown as a dotted line in the t_P–t_K plot (see Fig. 10). Figure 10 shows that only the Ba–Ti–O and Sr–Mo–O systems belong to area (B)

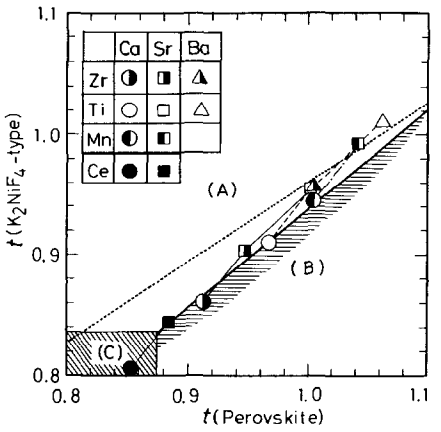

FIG. 10. Tolerance factor map. The tolerance factors of perovskites and K_2NiF_4 compounds are evaluated using the transition metal ionic radii with 6 coordinates and the alkaline earth ions with 12 and 9 coordinates, respectively. The field (A) represents an area in which both perovskite and K_2NiF_4 compounds stably exist, whereas in the field (B), K_2NiF_4 compounds are unstable against disproportionation: in the field (C), no perovskite nor K_2NiF_4 compound is stable. The solid line between the fields (A) and (B) was calculated using Eqs. (4) and (16) given in text.

under the assumptions $\alpha_P = \alpha_K$ and $\beta_P = \beta_K$. This is not consistent with experimental facts on the appearance of K_2NiF_4 compounds given in Fig. 9.

To account for features summarized in Fig. 9, the stabilization energy of K_2NiF_4 compounds were estimated so as to be within the upper limit of the enthalpy of formation for stable K_2NiF_4 compounds and the lower limit for unstable K_2NiF_4 compounds indicated in Fig. 6 by arrows. Numerically, this relation can be given as

$$\delta_K = 3[-65 + 400(1 - t_K)] \text{ kJ mole}^{-1}. \quad (16)$$

This is represented by a solid line in Fig. 10.

An interesting point in Fig. 10 is that only calcium systems enter region (B) in which a K_2NiF_4 phase should be unstable; with increasing radius of transition metal ions, Ca_2MO_4 and $Ca_3M_2O_7$ phases disappear sequentially and finally $CaMO_3$ disappears (region (C)). On the other hand, strontium and barium systems remain in region (A) and enter region (C) directly. These tendencies can be also found in the *A*–Ce–O system; in the Ca–Ce–O system, no K_2NiF_4 or perovskite phase is reported, whereas Sr_2CeO_4 and $SrCeO_3$ have both been reported.

This behavior, which is intrinsic to the calcium systems, can be ascribed to the relatively small size of calcium ions with 9 coordinates, which makes the tolerance factor of the A_2BO_4 phase relatively small. As Fig. 11 shows, the ionic radii decrease with decreasing coordination number. This shrinkage is more significant in calcium ion than in strontium or barium ions; as given in Table V the same tendency can be found in Pois' radii (*50, 51*). At a first glance, this implies that there may be some peculiarity with calcium ions. Even so, careful examination of the ionic radii–coordination number relation given in Fig. 11 suggests that the calcium ion may be normal from the ionic point of view, whereas strontium and barium show some deviation from purely ionic nature with decreasing coordination number. Since the empirical ionic radii are determined from the averaged ionic distance among actual crystals, they should include

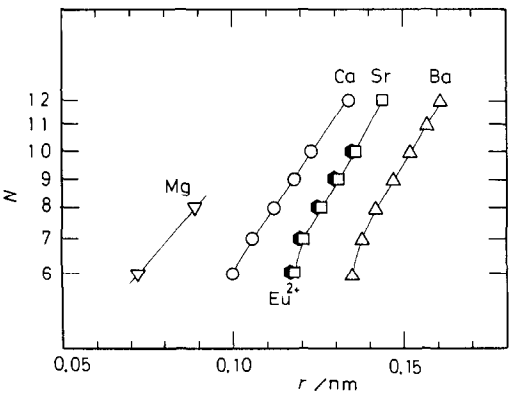

FIG. 11. Ionic radius as a function of coordination number for Mg, Ca, Sr, Ba, and Eu(II).

partly some information of chemical bonds and their strengths.

Some Remarks on Stability of K_2NiF_4 Compounds

Figure 6 shows that the stabilization energy per transition metal ion is higher for K_2NiF_4 compounds than for perovskites when a comparison is made at the same tolerance factor. Even so, the actual stability polygon for K_2NiF_4 compounds is quite narrow. This is due to the coordination number-dependent radii of alkaline earth ions which stabilizes perovskites more efficiently. The lower stability of K_2NiF_4 compounds gives rise to some problems in the experimental determination of phase relations.

For example, the present correlation for K_2NiF_4 compounds suggests that Sr_2MoO_4 may be stable at a reducing atmosphere as shown in Fig. 4. Actually, Lindblom and Rosen (*35*) succeeded in measuring EMFs associated with a phase combination of Sr_2MoO_4, Mo, and SrO, which corresponds to the following decomposition reaction of Sr_2MoO_4:

$$Sr_2MoO_4 = 2SrO + Mo + O_2(g). \quad (17)$$

On the other hand, Kamata *et al.* (*34*) observed the direct reduction of $SrMoO_3$ as

$$SrMoO_3 = SrO + Mo + O_2(g), \quad (18)$$

where Sr_2MoO_4 was not observed. As shown in Fig. 4, this contradicts the above EMF results. This discrepancy implies that some kinetic factor affects the dissociation reaction, since EMF measurements were made on mixtures containing Sr_2MoO_4 carefully prepared before measurements. In addition, Fig. 4 shows that the stability polygon of Sr_2MoO_4 is narrowed also by the presence of the Sr_3MoO_6 phase. Essentially the same discrepancy can be seen in the Ba–Mo–O system. Kamata *et al.* (*34*) observed the direction reduction of $BaMoO_3$ to BaO and Mo; however, the estimated

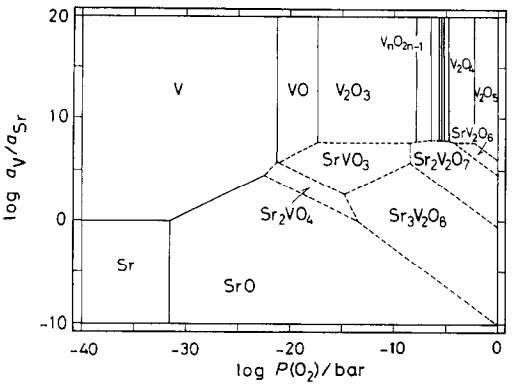

FIG. 12. Estimated chemical potential diagram of the Sr–V–O system at 1473 K. Some phases such as SrV_2O_4 were neglected.

thermodynamic properties of Ba_2MoO_5 and Ba_3MoO_6 given in Table IV imply some possibility that $BaMoO_3$ is not in equilibrium with the BaO and Mo phases.

The lower stability of K_2NiF_4 compounds has been observed also in the Sr–V–O system. Figure 12 shows the estimated chemical potential diagram of the Sr–V–O system at 1473 K; the thermodynamic properties of $SrVO_3$ and Sr_2VO_4 were estimated using the present correlations. The vertical width of the stability polygon for Sr_2VO_4 is narrower than that for $SrVO_3$. The known thermodynamic properties of calcium vanadates (*17*) suggest that $Sr_3V_2O_8$ is expected to have a large stabilization energy. The presence of this phase cuts off the oxidizing side of the stability polygon for Sr_2VO_4 and makes it difficult to obtain the pure phase experimentally (*52*).

V. Oxygen Nonstoichiometry

The present study reveals that the chemical thermodynamic features of the K_2NiF_4 phase can be interpreted in terms of coordination number-dependent ionic radius, and that the empirical ionic radii determined by Shannon (*48*) include information on ener-

TABLE V

EFFECTIVE IONIC RADII (GIVEN IN NM) OF ALKALINE EARTH IONS WITH COORDINATION NUMBERS (CN) OF 9 AND 12

Ion	Shanon			Pois	
	CN = 12	CN = 9	Ratio[a]	CN = 9	ratio[b]
Ca^{2+}	0.134	0.118	(0.88)	0.1147[c]	(0.86)
Sr^{2+}	0.144	0.131	(0.91)	0.1268	(0.88)
Ba^{2+}	0.161	0.147	(0.91)	0.1418	(0.88)

[a] Ratio of Shannon's radii of coordination number 12 to that of coordination number 9.

[b] Ratio of Shannon's radii for CN = 12 to Pois's radii for CN = 9.

[c] Ionic distance between oxide ions and alkaline earth ions with nine coordinates—oxide ionic radius (0.14 nm).

getics as well as chemical bonds. This suggests that similar considerations based on ionic radii can be applied to analyze the formation of various lattice defects.

For example, when oxygen vacancies are formed in perovskite structure, the coordination numbers of *A*-site as well as *B*-site ions decrease. However, the situation is more complicated than in the Ruddlesden–Popper series in which *B*-site cations remain in the same octahedral configuration. Provided that *B*-site cations in perovskites are reduced to the valence state of 3+ and oxygen vacancies are arranged randomly, the coordination number of *B*-site and of *A*-site cations become 5 and 10, respectively; this is the case for $SrTiO_{2.5}$. Alternatively, oxygen vacancies can be ordered in several different ways (*6*); in a brownmillerite-type structure, the combination of octahedra and tetrahedra is preferential, whereas the square-pyramidal configuration having 5 coordinates is preferential in $CaMnO_{2.5}$ (*53*). These ordering structures should be therefore related to the difference in site preferential energies of M^{3+} and M^{4+} ions having different electron configurations. This makes it quite difficult to find dominant factors determining the degree of oxygen nonstoichiometry throughout the transition metal series.

When comparison is made among systems with the same *B*-site ions, changes associated with *B*-site cations can be expected to be essentially the same, because the site preferential energies are not affected greatly by *A*-site cations. The present analytical results thus lead to an expectation that the calcium perovskites may have a smaller amount of oxygen vacancies than strontium analogs. Note that the strontium perovskites ($SrTiO_3$, $SrFeO_3$, $SrMnO_3$) actually show a large oxygen nonstoichiometry. For example, $SrTiO_{2.5}$ (*15*) maintains the cubic perovskite lattice, indicating that the oxygen vacancies are arranged without ordering; note that $CaTiO_{2.5}$ has not been reported (*6*). For the *A*–Mn–O system, both $SrMnO_{3-x}$ and $CaMnO_{3-x}$ have been reported. Although both phases show significant oxygen nonstoichiometry, the extent (x) is larger in $SrMnO_{3-x}$ than in $CaMnO_{3-x}$ at the same temperature (*54, 55*). Furthermore, the nonstoichiometry of $SrFeO_{3-x}$ is quite significant, whereas many attempts have been made to synthesize $CaFeO_{3-x}$ without success except for specialized experiments (*56*). This can be ascribed to the shift of the stability area of $CaFeO_{3-x}$ to the oxidizing side because of (1) the small stabilization energy of $CaFeO_3$ and of (2) the small number of oxygen vacancies.

A plausible effect of covalency in stabilizing Fe^{4+} ions in perovskites has been pointed out to explain the existence of $SrFeO_{3-x}$ and other phases (*57*). Note also that many strontium perovskites with oxygen nonstoichiometry exhibit metallic conductivities whereas the calcium analogs have localized electrons (*6*). This is consistent with the present correlation based on the empirical radii, which should reflect the difference in chemical bonds between Ca and Sr oxides. Investigations to represent in chemical thermodynamic terms the oxygen

nonstoichiometry in the A–M–O systems are now in progress for A = Ca, Sr and M = Mn, Fe, Co.

Qualitatively speaking, the present discussion can be summarized by saying that strontium can provide oxygen vacancies, whereas calcium can inhibit the formation of oxygen vacancies. It is of interest to see how this property can be applied to technological problems, in which many dopants are added to form complicated multicomponent materials. For example, Sakabe (*58*) found that calcium-doped $BaTiO_3$ having a composition of $\{(BaO)_{1-x}(CaO)_x\}_{1.01}TiO_2$ (x = 0.01–0.2) is quite effective in inhibiting the reduction of $BaTiO_3$ during firing in a reducing atmosphere together with Ni. He ascribed this phenomenon to the B-site substitution by Ca. The present results imply that the calcium ions occupying A sites may also work to inhibit the formation of oxygen vacancies; note that strontium or magnesium do not work well. This example indicates that the difference in abilities of vacancy formation between calcium and strontium may hold even in multicomponent systems.

VI. Conclusions

Thermodynamic data for double oxides in the alkaline earth–transition metal–oxygen systems have been assessed and estimated. The chemical potential diagrams have been constructed to clarify the stability area of perovskites and related phases. It has been found that the correlation between tolerance factor and enthalpy of formation among perovskites is quite useful to understand why no perovskite phase is found in the Sr–W–O system nor in the Eu–Mo–O system. The stability of K_2NiF_4 compounds has been examined in terms of the thermodynamic properties of dissociation reaction of K_2NiF_4 compounds into perovskites and alkaline earth monoxide. This makes it possible to derive a linear correlation for K_2NiF_4 compounds. These are thermodynamically consistent with the appearance–disappearance of K_2NiF_4 and other Ruddlesden–Popper phases; that is, the calcium K_2NiF_4 compound with the large transition metal ions tends to become unstable with increasing radius of transition metal ions. A similar consideration based on the ionic radii may provide a good explanation for why strontium perovskites may have a large amount of oxygen vacancies when compared with the analogous calcium perovskites.

References

1. J. B. Goodenough, and J. M. Longo, *in* "Magnetic Oxides and Related Oxides," Vol. 4a, Ch. 3, pp. 126–314, Landolt-Bernstein (1970).
2. S. Nomura, *in* "Magnetic Oxides and Related Oxides," Vol. 4a, pp. 368–520, Landolt-Bernstein (1978).
3. F. S. Galasso, "Structure, Properties and Preparation of Perovskite-Type Compounds," Pergamon, Elmsford, NY (1969).
4. J. B. Goodenough, *J. Appl. Phys.* **37,** 1415 (1966).
5. P. Ganguly and C. N. R. Rao, *J. Solid State Chem.* **53,** 193–216 (1984).
6. C. N. R. Rao, J. Gopalakrishnan, and K. Vidyasagar, *Indian J. Chem. Sect. A* **23,** 265–284 (April 1984).
7. L. R. Morss, *J. Less-Common Met.* **93,** 301 (1983).
8. A. Navrotsky, *in* "Structure and Bonding in Crystals," (M. O'Keefe and A. Navrotsky, Eds.), Vol. II, pp. 71–93, Academic Press, New York (1981).
9. E. Takayama-Muromachi, and A. Navrotsky, *J. Solid State Chem.* **72,** 244 (1988).
10. S. N. Ruddlesden and P. Popper, *Acta Crystallogr.* **11,** 178 (1969).
11. H. Yokokawa, T. Kawada, and M. Dokiya, *J. Am. Ceram. Soc.* **72,** 152 (1989).
12. H. Yokokawa, T. Kawada, and M. Dokiya, *J. Am. Ceram. Soc.* **72,** 2104 (1989).
13. H. Yokokawa, N. Sakai, T. Kawada, and M. Dokiya, *J. Am. Ceram. Soc.* **73,** 649 (1990).
14. H. Yokokawa, N. Sakai, T. Kawada, and M. Dokiya, "Stability and Reaction of Perovskite Materials in SOFCs; Proceedings, SOFC Nagoya, Nov. 13–14, 1989," pp. 118–134, Science House Co., Ltd., Tokyo, 1990.
15. H. Yokokawa, N. Sakai, T. Kawada, and M. Dokiya, *J. Electrochem. Soc.*, **138,** 1018 (1991).
16. H. Yokokawa, N. Sakai, T. Kawada, and M. Dokiya, "Thermodynamic Stabilities of Perovskite Oxides for Electrodes and Other Electro-

chemical Materials," presented in workshop on "Ceramic Conductors for Solid State Electrochemical Devices," May 12–15, 1991, Snowbird, Utah.

17. D. D. WAGMAN, W. H. EVANS, V. B. PARKER, R. H. SCHUMM, I. HALOW, S. M. BAILEY, K. L. CHURNEY, AND R. L. NUTTALL, "The NBS Table of Chemical Thermodynamic Properties," *J. Phys. Chem. Ref. Data* **11**(Suppl. 2) (1982).
18. M. W. CHASE, JR., C. A. DAVIES, J. R. DOWNEY, JR., D. J. FRURIP, R. A. MCDONALD, AND A. N. SYVERUD, "JANAF Thermodynamical Tables," 3rd ed., *J. Phys. Chem. Ref. Data* **14**(Suppl. 1) (1985).
19. V. P. GLUSHKOV, L. V. GURVICH, G. A. BERGMAN, I. V. VEITZ, V. A. MEDVEDEV, G. A. KHACHKURUZOV, AND V. A. YUNGMAN, "Thermodynamic Data for Individual Substances," High Temperature Institute, State Institute of Applied Chemistry, National Academy of Sciences of U.S.S.R., Moscow, (1982).
20. The Society of Calorimetry and Thermal Analysis, Japan, "Thermodynamic Database MALT," Kagakugijutsusha, Tokyo, (1986); see also H. YOKOKAWA, S. FUJIEDA, AND S. YAMAUCHI, MALT: Materials Oriented Little Thermodynamic Database for Personal Computer, *in* "Data Handling and Dissemination."
21. I. BARIN, O. KNACKE AND O. KUBASCHEWSKI, "Thermodynamic Properties of Inorganic Substances," VerlagStahleisen (1976).
22. O. KUBASCHEWSKI AND C. B. ALCOCK, "Metallurgical Thermochemistry," 5th ed. Pergamon, Oxford, (1979).
23. I. BARIN, "Thermochemical Data of Pure Substances," VCH Verlagsgesellschaft, Weinheim, (1989).
24. O. KUBASCHEWSKI, ORTRUD KUBASCHEWSKI-VON GOLDBECK, P. ROGL, H. F. FRANZEN, "Titanium: Physico-Chemical Properties of Its Compounds and Alloys," Atomic Energy Review, Special Issue No. 9, IAEA, Vienna, (1983).
25. C. B. ALCOCK, K. T. JACOB, S. ZADOR, ORTRUD KUBASCHEWSKI-VON GOLDBECK, H. NOWOTNY, K. SEIFERT, AND O. KUBASCHEWSKI, "Zirconium: Physico-Chemical Properties of Its Compounds and Alloys," Atomic Energy Review, Special Issue No. 6, IAEA, Vienna, (1976).
26. P. J. SPENCER, ORTRUD KUBASCHEWSKI-VON GOLDBECK, R. FERRO, R. MARAZZA, K. GIRGIS, AND O. KUBASCHEWSKI, "Hafnium: Physico-Chemical Properties of Its Compounds and Alloys," Atomic Energy Review, Special Issue No. 8, IAEA, Vienna, (1981).
27. E. H. P. CORDFUNKE AND R. J. M. KONIGS (Eds.) "Thermodynamical Data for Reactor Materials and Fission Products," North-Holland, Amsterdam, 1990.
28. R. R. BROWN AND K. BENNINGTON, *Thermochim. Acta* **106,** 183–190 (1986).
29. V. A. LEVITSKII, *J. Solid State Chem.* **25,** 9–22 (1978).
30. S. PIZZINI AND R. MORLOTTI, *J. Chem. Soc. Farad. Trans.* **68,** 1601 (1972).
31. K. NAGARAJAN, R. SAHA, R. BABU, AND C. K. MATHEWS, *Thermochim. Acta* **90,** 297–304 (1985).
32. A. S. L'VOVA AND N. N. FEODOS'EV, *Russ. J. Phys. Chem.* **38,** 14 (1964).
33. A. S. L'VOVA AND N. N. FEODOS'EV, *Russ. J. Phys. Chem.* **39,** 1091 (1965).
34. K. KAMATA, T. NAKAMURA, AND T. SATA, *Mater. Res. Bull.* **10,** 373 (1975).
35. B. LINDBLOM AND E. ROSEN, *Acta Chem. Scand. A* **40,** 452 (1986).
36. O. KUBASCHEWSKI, T. HOSTER, R. SCHLIM, *Ber. Bunsenges. Phys. Chem.* **85,** 367 (1981).
37. L. A. ZHARKOVA, V. I. LAVRENT'EV, Y. I. GERASIMOV, AND T. N. REZNKHINA, *Dokl. Akad. Nauk SSSR* **131,** 872 (1960).
38. V. A. LEVITSKII AND Y. Y. SCOLIS, *J. Chem. Thermodyn.* **6,** 1181 (1974).
39. V. A. LEVITSKII, YU. HEKIMOV, AND JA. I. GERASSIMOV, *J. Chem. Thermodyn.* **11,** 1075 (1979).
40. A. S. ALIKHANHAN, K. N. MARUSHKIN, J. H. GREENBERG, V. B. LAZAREV, AND V. I. GORGORAKI, *J. Chem. Thermodyn.* **20,** 1035 (1988); see also A. S. ALIKHANYAN, K. N. MARUSHKIN, YA. KH. GRINBERG, V. B. LAZAREV, AND V. I. GORGORAKI, *Russ. J. Inorg. Chem.* **33**(6), 883 (1988).
41. A. N. BLOCH AND G. C. SCHATTLEMAN, *in* "Structure and Bonding in Crystals," M. O'Keefe and A. Navrotsky, Eds.), Vol. I, pp. 49–72, Academic Press, New York (1981).
42. A. ZUNGER, *in* "Structure and Bonding in Crystals" (M. O'Keefe and A. Navrotsky, Eds.), Vol. I, pp. 73–135, Academic Press, New York (1981).
43. P. VILLARS, K. MATHIS, AND F. HULLINGER, *in* "The Structure of Binary Compounds," (F. R. de Boer and D. G. Pettifor, Eds.), pp. 1–103, North-Holland, Amsterdam (1989).
44. J. C. PHILLIPS, "Treatise on Solid State Chemistry," Vol. I, pp. 1–41 (1971).
45. W. SLOUGH, "A Comparison of Methods Available for the Estimation of Enthalpies of Formation for the Double Oxides Systems," NPL Report Chem., Vol. 25, (1973).
46. J. GOUDIAKAS, R. G. HAIRE, J. FUGER, *J. Chem. Thermodyn.* **22,** 577 (1990).
47. L. A. REZNITSKII, *Neorg. Mater.* **14,** 2127 (978).
48. R. D. SHANNON, *Acta Crystallogr. Sect. A* **32,** 751 (1976).
49. G. J. MCCARTHY, *Mater. Res. Bull.* **6,** 31 (1971).
50. P. POIS, *J. Solid State Chem.* **31,** 95 (1980).
51. P. POIS, *C. R. Acad. Sci. Paris* **268,** 1139 (1969).

52. M. J. Rey, Ph. Dehaudt, J. C. Joubert, B. Lambert-Andron, M. Cyrot, and F. Cyrot-Lackmann, *J. Solid State Chem.* **86,** 101 (1990).
53. A. Reller, D. A. Jefferson, J. M. Thomas, R. A. Beyerlein, and K. R. Poepplemeier, *J. Chem. Soc. Chem. Commun.*, 1378 (1982).
54. H. Taguchi, *Phys. Status Solidi A* **88,** K79 (1985).
55. T. Negas and R. S. Roth, *J. Solid State Chem.* **1,** 409 (1970).
56. F. Kanamaru, H. Miyamoto, Y. Mimura, M. Koizumi, M. Shimada, S. Kume, and M. Shin, *Mater. Res. Bull.* **5,** 257 (1970).
57. P. K. Gallagher, J. B. MacChesney, and D. N. E. Buchanan, *J. Chem. Phys.* **45,** 2466 (1961).
58. Y. Sakabe, *Ceram. Bull.* **66,** 1338 (1987).